PAPER

Check for updates

Exploring the dynamics of DNA nucleotides in graphene/h-BN nanopores: insights from *ab initio* molecular dynamics†

Ali Kiakojouri,[a] Irmgard Frank[b] and Ebrahim Nadimi ✪ *[a]

Nanopore devices based on graphene and h-BN heterostructures show outstanding electrical and physical characteristics for high throughput label-free DNA sequencing. On top of their suitability for DNA sequencing with the ionic current method, G/h-BN nanostructures are promising for DNA sequencing by employing the in-plane electronic current. The influence of the nucleotide/device interaction on the in-plane current has been widely explored for static-optimized geometries. Therefore, it is essential to investigate the dynamics of the nucleotides within the G/h-BN nanopores to gain a comprehensive view of their interaction with the nanopores. In this study, we investigated the dynamic interaction between nucleotides and nanopores in horizontal graphene/h-BN/graphene hetero-structures. The insulating h-BN layer, where the nanopores are implemented, changes the in-plane charge transport mechanism into the quantum mechanical tunneling regime. We employed the Car–Parrinello molecular dynamics (CPMD) formalism to investigate the interaction of the nucleotides with nanopores in a vacuum as well as in an aqueous environment. The simulation was performed in the *NVE* canonical ensemble with an initial temperature of 300 K. The results indicate that the interaction between the electronegative ends of the nucleotides and the atoms at the nanopore edge is essential for the dynamic behavior of the nucleotides. Moreover, water molecules have a substantial effect on the dynamics and interactions of the nucleotides with nanopores.

Introduction

DNA sequencing is a means to decipher the genetic information in every living cell, which is essential in many aspects, particularly in diagnosing and curing diseases. Moreover, synthesized strands of DNA provide a medium for data storage, which will be read by DNA sequencing methods as well. Recent development in the next-generation sequencing methods (NGS) is based on label-free and high throughput sequencing devices, which are cheaper and faster than previous generations such as the Sanger sequencing method.[1] Recently, nanotechnology-based devices including devices based on nanopore structures have attracted enormous attention as a promising and affordable approach for fast and reliable DNA sequencing. In nanopore-based devices, the double or single-strand DNA is driven through a nanopore by an external electric field. As different nucleotides are passing through the nanopore, the sequencing process can be achieved by measuring the modulation of the ionic current that passes through the membrane.[2]

The nanopore-based sequencing devices are realized either in biological materials, such as α-haemolysin[3] or in solid-state materials. The limitations of early biological nanopores, such as high manufacturing cost, low signal-to-noise ratio, and instability at high voltages, pave the way for solid-state nano-pores as the most viable option. Numerous solid-state devices based on SiO_2,[4] Al_2O_3,[5] HfO_2,[6] and Si_3N_4[7] crystals have been developed, where the ionic current modulation is utilized for DNA sequencing. Solid-state nanopores have various advantages, such as high durability and stability as well as low manufacturing complexity. However, they still suffer from important issues such as controlling the translocation speed of the nucleotides as well as the required resolution for single nucleotide detection.[8] Recent studies reveal that single-atomic-layer or two-dimensional (2D) materials, such as graphene, can effectively alleviate these drawbacks.[9]

The thickness of single-atomic-layer materials is in the same range as the distance between the neighboring nucleotides in a DNA strand. This makes the detection of a single nucleo-tide with high spatial resolution possible. The feasibility of

[a] *Center for Computational Micro and Nanoelectronics, Faculty of Electrical Engineering, K. N. Toosi University of Technology, 16317-14191 Tehran, Iran. E-mail: nadimi@kntu.ac.ir*

[b] *Theoretische Chemie, Universität Hannover, Callinstr. 3A, 30167 Hannover, Germany*

† Electronic supplementary information (ESI) available. See DOI: https://doi.org/10.1039/d3cp00416c

fabricating nanometer-sized holes in 2D materials with novel methods has been reported.[10,11] Consequently, numerous studies have been conducted on the feasibility of DNA sequencing with different 2D materials such as graphene,[12,13] MoS_2,[14,15] and hexagonal boron nitride (h-BN).[16] Graphene, the 2D allotrope of carbon, has been widely studied for DNA sequencing due to its unique physical and electrical characteristics. The low thickness of graphene (0.35 nm) along with high mechanical strength and ionic blockage ability, make it an attractive choice for ionic current sequencing approaches. The electrical conductivity of graphene provides an alternative method, in which the modulation of in-plane electrical current is also employed as a sequencing signal.[17] Several theoretical and experimental studies have been conducted to study graphene-based nanopores for NGS methods.[18–20] For instance, the possibility of single-molecule detection with the high spatial resolution has been reported in an experimental study.[19] Another study reported the application of functionalized graphene nanopores in DNA sequencing based on ionic current modulation.[20]

While graphene nanopores are indicated to have great advantages in DNA sequencing, some drawbacks have also been reported, particularly when the in-plane electrical current is considered as the sequencing signal. Graphene is a zero bandgap material with high conductivity on the surface, which puts some limits on the sensitivity of the in-plane electronic current toward different nucleotides.[17] In addition, low mechanical stability at nanopore edges results in a high signal-to-noise ratio (SNR) compared to other solid-state nanopores such as Si_3N_4.[21] Moreover, strong π–π interaction with nucleotides leads to DNA adherence at the graphene nanopore edges, which hinders the translocation of the DNA strand and leads to nanopore clogging.[22]

Several modifications to the graphene nanopore have been proposed to overcome the challenges while maintaining its advantages. Fabricating hybrid heterostructures consisting of graphene and similar 2D nanostructures, particularly h-BN, has been considered as a practical solution.[23,24] The atomic structure of h-BN is very similar to graphene with a small lattice mismatch (less than 1.5%). Experimental studies have shown the successful fabrication of single-layer hybrid graphene and h-BN (G/h-BN) heterostructures with atomic precision at the interface.[25] Despite the structural similarity between h-BN and graphene, h-BN is insulating with a direct bandgap of ∼6.8 eV.[26]

The suitability of h-BN nanopores for DNA sequencing with the single-molecule resolution has been proven experimentally.[27] The ionic character of B–N bonding in h-BN facilitates the passivation of nanopore edge atoms, which is essential to modify the interaction between the nucleotides and the nanopore and reduces the possibility of nanopore clogging.[28,29] Moreover, it has been revealed that the amount of flicker noise caused by h-BN nanopore edges is substantially lower than its graphene counterpart.[28]

In G/h-BN heterostructures, the advantages of both materials are synergistically employed to design an attractive nanostructure for both ionic and electronic sequencing applications.

Several theoretical studies have employed density functional theory (DFT) and non-equilibrium Green's function (NEGF) formalisms to investigate the performance of G/h-BN-based nanopores for such applications.[30–32] It has been shown that at the edge of graphene and h-BN nanoribbons, there are one-dimensional conductive states.[32] The current at this interface is highly sensitive to the adjacent nucleotides, which translocate through the nanopore, fabricated a few atomic layers away from the interface. Also, it has been reported that placing insulating h-BN within graphene layers changes the mechanism of the in-plane current from band conductivity to quantum mechanical tunneling. This tunneling current is highly sensitive to the modulation of the potential barrier caused by the translocation of nucleotides within the h-BN nanopore. Therefore, employing tunneling current in the channel can lead to substantially high sensitivity compared to the band current mechanism, which is the case in graphene nanopores.[33]

However, most of these DFT studies find some optimized geometries for the nucleotides in the nanopore and consequently consider a static picture of the nucleotides within the nanopore. The interactions between nucleotides and nanopores are then calculated for these relaxed geometries. Despite the promising findings, some questions remain open about the dynamics of the interaction between nucleotides and graphene or G/h-BN nanopores. In fact, the fluctuation of the nucleotides within the nanopore leads to a non-negligible impact on the interaction and the sensing signal. Therefore, the understanding of the dynamics between nucleotides and nanopores is a crucial issue. Classical or *ab initio* molecular dynamics (AIMD) have been widely employed to investigate the dynamic motion of DNA strands through the graphene and G/h-BN nanopores.[34–36] However, such studies for G/h-BN heterostructure-based nanopores are scarce. Another critical factor is the impact of the aqueous environment or water molecules on the dynamics of the nucleotides within the nanopores. Classical and QM/MM molecular dynamics have been conducted in several studies to describe the impact of an aqueous environment on the performance of graphene nanopores.[37,38] It has been reported that the water molecules have no tendency to interact with the graphene or DNA strand, and their effect is similar to a gating voltage, in the case of in-plane electronic current. However, the impact of water molecules on the G/h-BN nanopores still needs to be investigated.

In the present work, we explore the dynamic interaction between different nucleotides (dAMP, dCMP, dTMP, and dGMP) and the proposed G/h-BN/G and pure graphene nanopores. The relaxed geometries of the nucleotides within the nanopores are considered as the starting point for molecular dynamics calculations. The proposed nanostructures are arranged so that the h-BN layer is sandwiched between two graphene layers, as depicted in Fig. 1. The h-BN layer acts as an insulating channel, which changes the mechanism of the in-plane current to the quantum mechanical tunneling regime. We employed *ab initio* molecular dynamics (AIMD) based on the state-of-the-art Car-Parrinello molecular dynamic (CPMD) formalism to investigate the dynamic interaction of the nucleotides. Graphene nanopore is
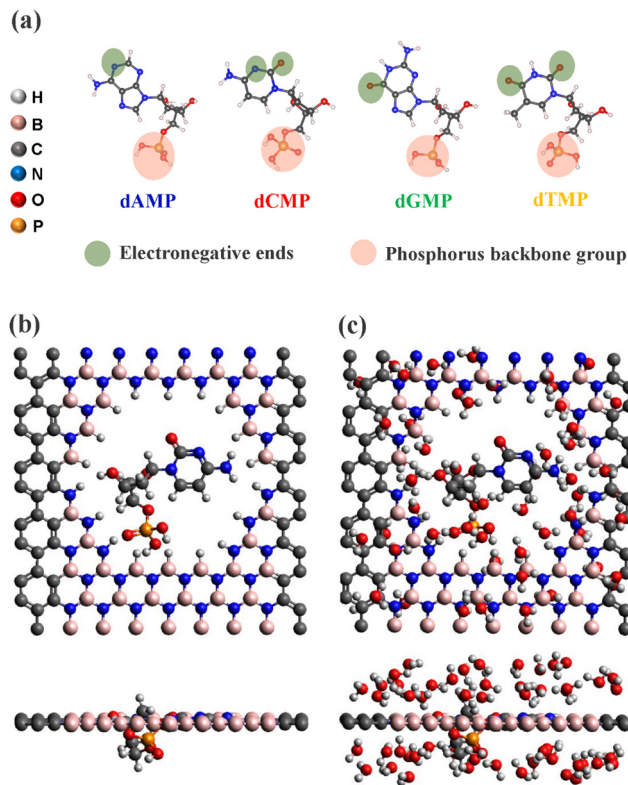
This journal is © the Owner Societies 2023

Phys. Chem. Chem. Phys., 2023, **25**, 13452–13464 | **13453**

Fig. 1 (a) The nucleotides of DNA structure: dAMP, dCMP, dGMP, and dTMP. (b) G/h–BN/G heterostructure with 7 layers of h–BN (G7BN) with dCMP, in vacuum environment as well as (c) in aqueous environment.

considered as the reference structure and the results are compared with the findings for different G/h-BN/G nanopores. We also studied systems with and without an aqueous environment to assess the impact of water molecules.

Model and computational details

In order to model the G/h-BN/G heterostructure a supercell of 144 atoms with dimensions of 20.97×20.71 Å is considered. A nanopore with a diameter of 12 Å is implemented in the middle of the supercell and the dangling bonds at the edge are passivated with hydrogen atoms. Fig. 1(a) shows the four DNA nucleotides, including dAMP, dCMP, dTMP, and dGMP, which are individually modeled and optimized. As depicted in Fig. 1(b), the nucleotides are horizontally aligned within the nanopore at their initial positions. It means that the aromatic rings of the nucleotides within the nanopores are aligned with the surface of graphene and h-BN membranes. Two samples of G/h-BN/G nanopores with 5 and 7 rows of h-BN (G-5BN and G-7BN), plus a pure graphene nanopore as a reference structure, were considered for this study. In pure graphene, the edge of the nanopore consists of C atoms (passivated by H atoms), the edges of the G-5BN nanopore consist of B, C, and N atoms, whereas the G-7BN nanopore edges consist of only B and N atoms. It will be shown that these differences lead to different interactions between the nucleotides and different nanopores. The structure

of the G-7BN nanopore is illustrated in Fig. 1(b), while the G-5BN and graphene nanopore structures are shown in Fig. S1 (ESI†).

For the molecular dynamics calculations, we employed the CPMD program suite, a DFT-based *ab initio* molecular dynamics code with an implementation of the Car–Parrinello (CP) molecular dynamics.[39,40] This method is applied to the optimization of isolated nucleotides and nanopore structures, equilibrating the water molecules as well as the dynamics of four nucleotides in different nanopores. All inner electrons are represented by Troullier–Martins norm-conserving pseudo-potentials.[41] The PBE version of the generalized-gradient-approximation, GGA-PBE[42] was chosen along with the Grimme dispersion correction[43] to account for the long-range van der Waals interactions. The plane-wave cutoff was set to 70 Ry in all the calculations. In the molecular dynamics part of the calculations, the simulation time step and the fictitious electron mass were set to 0.048 fs (2 a.u.) and 200 a.u., respectively. The vertical dimension of the supercells was set to 15 Å and 10 Å for vacuum and solvent environments, respectively. Previous studies have illustrated that the applied temperature has a substantial impact on the stability and physical characteristics of 2-D structures.[44] Therefore, determining suitable temperatures for molecular dynamics simulations is essential for obtaining accurate results. The presence of water molecules in the environment and the organic nature of nucleotides in DNA strands are two deciding factors that limit the temperature range that can be practically carried out in the simulation. Considering these factors, performing the molecular dynamics simulation in the temperature range of around 293–365 K is feasible and similar to real-world sequencing scenarios. Therefore, the simulation was performed in the *NVE* canonical ensemble with an initial temperature of 300 K. Also, simulations in the solvent environment were carried out at 350 K to study the impact of a subtle change in temperature on stability and interactions. The initial distribution of water molecules in the aqueous environment was extracted from the Solvate extension of the VMD software package.[45] After submerging the nanopore heterostructure into the aqueous environment, excessive water molecules were removed to maintain the total density of the system in the range of 1 g cm^{-3}. Fig. 1c illustrates the G-7BN nanopore and the dCMP nucleotide in the solvent environment. The radial distribution functions (RDF) of O–O bonds as well as H–O bonds are depicted in Fig. S2 (ESI†), which approves the well-known distribution of water molecules in the liquid phase.[46]

The binding energy between nucleotides and nanopores at some selected time steps was calculated by evaluating the energies according to the following equation:

$$E_{\text{B}} = E_{\text{pore+nucl}} - (E_{\text{pore}} + E_{\text{nucl}}) \qquad (1)$$

Here, E_{B} is the binding energy, $E_{\text{pore+nucl}}$ is the total energy of the system containing nucleotide and nanopore, E_{pore} is the total energy of the system when a nucleotide is removed, and E_{nucl} represents the energy of the isolated nucleotide. For the calculation of the binding energy in an aqueous environment

the same equation was used, where the fixed geometries at each time step were considered after removing all water molecules from the supercell.

For more details on the interaction between nucleotides and nanopores, we also evaluated the charge transfer between the parts of the system as well as the locally projected density of states (LDOS). These calculations are more easily done in a DFT implementation with a local atomic orbital basis set. Therefore, we employed the SIESTA package[47] to extract these data. Some snapshots were selected from the molecular dynamics simulations, and then the atomic coordinates of the whole structure were extracted from them. Then, the extracted atomic coordinates were imported to the SIESTA suite as the fixed geometries to evaluate the charge transfer and LDOS. Troullier–Martins norm-conserving pseudopotentials and the van der Waals corrected GGA-PBE functional were used in SIESTA calculations, too. The energy mesh cutoff for real space sampling is set to 300 Ry, and the first Brillouin zone was sampled according to the Monkhorst–Pack scheme with a $5 \times 5 \times 1$ k-point grid. A basis set at the level of double-zeta plus polarization (DZP) was employed for all the atoms.

Results and discussion

The interactions between the nucleotides and graphene as well as G/h-BN nanopores were studied by AIMD simulations. The calculations were performed for 2.4 ps (50 000 time per steps) in different environments. Analyzing the extracted data shed light on the dynamic behavior of the nucleotides within the nanopores. As an example of the outcomes, Fig. 2 shows three snapshots corresponding to the initial, middle, and final time steps of the calculations for dCMP and dGMP nucleotides within the G7BN nanopore in a vacuum environment. The snapshots for dAMP and dGMP are also depicted in Fig. S3 (ESI†) these results reveal that, while dCMP tends to remain in the nanopore, dGMP has been pushed out from the nanopore as a result of the interaction with the nanopore.

Similar to the results in Fig. 2, the calculations for all nucleotides and nanopores in a vacuum as well as in an aqueous environment show different dynamic patterns. In order to compare the different behaviors of the nucleotides, it is necessary to extract some numbers, which explain the interactions in terms of geometry and bonding between nucleotides and the nanopores. To this end, three bonding or geometric parameters were calculated and extracted for all samples during the whole 50 000 time steps of the AIMD simulations.

Previous studies[32,33] revealed that the main part of the interaction between the nucleotides and the nanopore is due to the electronegative active ends of every single nucleotide. The second source of interaction is between the backbone of the single-strand DNA and the edge of the nanopores. Therefore, the first parameter was chosen as the distance between the electronegative ends of the nucleotides and the passivating hydrogen atoms at the edge of the nanopore. In each time-step, the closest hydrogen atom at the nanopore
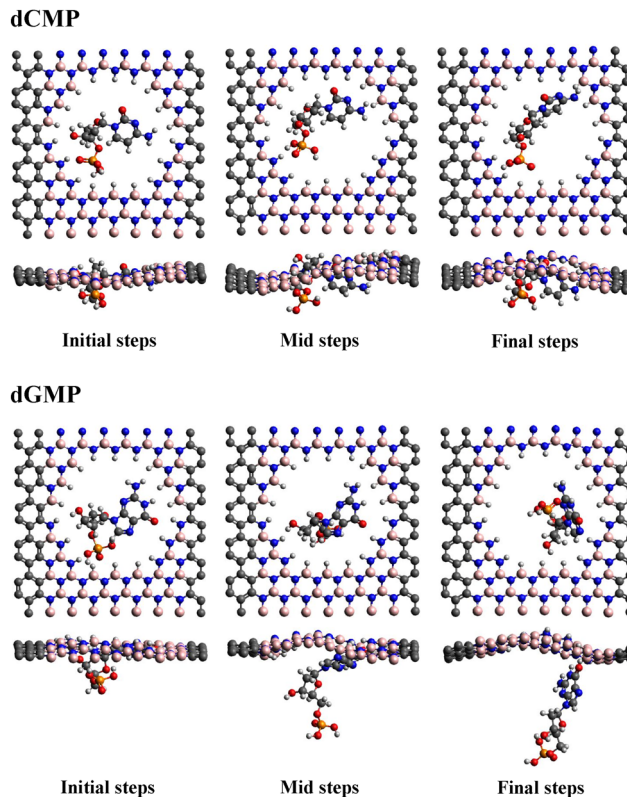

dCMP

Initial steps   Mid steps   Final steps

dGMP

Initial steps   Mid steps   Final steps

Fig. 2 dCMP and dGMP interaction with G7BN nanopore at initial, middle, and final time-steps of AIMD simulation.

edge was considered for the calculation of the distance. Measuring this distance during the movement and rotation of the nucleotides within the nanopore reveals important information about the dynamics of different nucleotides. Fig. 3 depicts this distance for four nucleotides within a graphene nanopore in a vacuum environment. For dAMP the active electronegative atom is nitrogen, and dCMP has oxygen and nitrogen electronegative atoms. Also, dGMP and dTMP have one and two oxygen atoms as their electronegative active end, respectively.

In a vacuum environment, the distance between electronegative ends and hydrogen atoms shows the characteristic bond length of hydrogen bonds (H-bond) for several time steps. However, the breaking of H-bonds was also observed due to the rotation or displacement of the nucleotides. dCMP, dGMP, and dTMP showed relatively stable H-bonds, which break but are established again during the AIMD simulation time. In contrast, the interaction of dAMP with the graphene nanopore forces the nucleotide out of the nanopore and the H-bond breaks without any reconnection up to the end of the AIMD simulation. This example shows that the distance between the electronegative ends and the hydrogen atoms at the nanopore edge can be considered a semiquantitative measure to explain the dynamic behavior of the nucleotides within the nanopores.

In the same way, the second interaction metric is considered the minimum distance between the backbone of the nucleotides and hydrogen atoms at the edge of the nanopores. More precisely,

This journal is © the Owner Societies 2023

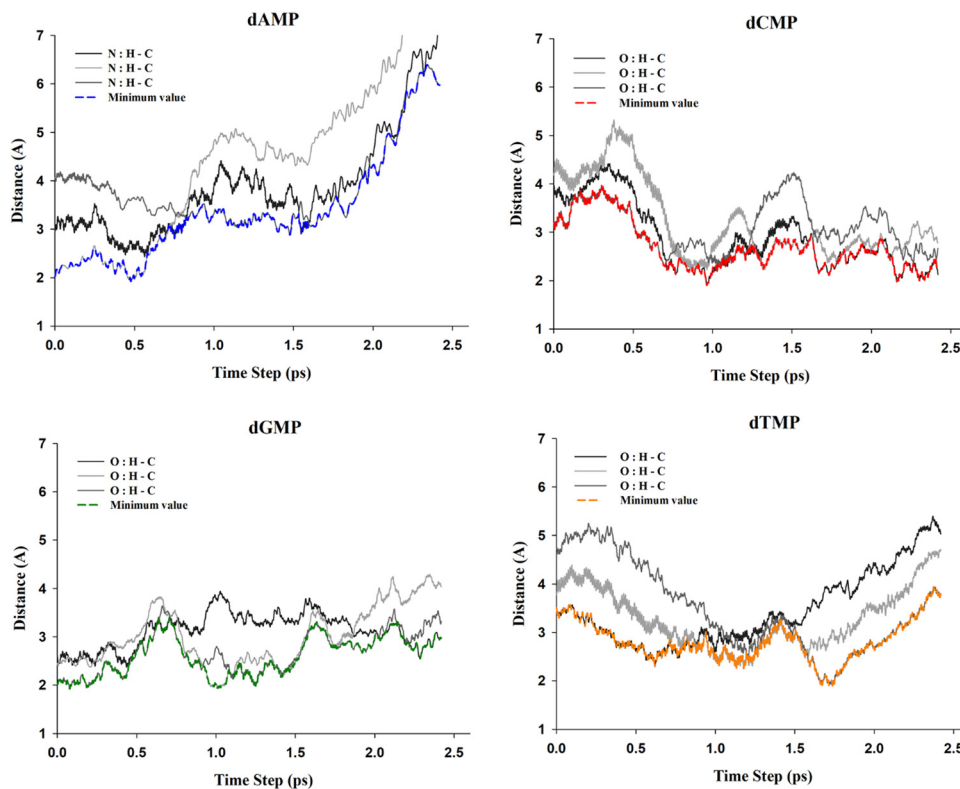*Phys. Chem. Chem. Phys.*, 2023, **25**, 13452–13464 | **13455**

Fig. 3 The distance between the hydrogen atoms at the edges of the graphene nanopore and the electronegative active ends of dAMP, dCMP, dGMP, and dTMP in vacuum environment. The minimum distance is plotted as a colored line.

the distance between the free oxygen of the backbones and the nearest hydrogen available at the nanopore edge was calculated throughout the simulation process. Apart from the interaction of the nucleotides with the nanopore edge, the average perpendicular or out-of-plane movement (z-direction) of the molecules relative to the surface of graphene or h-BN is also an important parameter. This parameter shows whether the nucleotide is stable within the nanopore or tends to move out of the nanopore. This movement is quantified by calculating the trajectory of the z-component related to the phosphor atom in the backbone and a chosen carbon atom, illustrated in Fig. S4 (ESI†) in the head of the nucleotide. This set of data not only shows the tendency of the nucleotides to leave the nanopore but also gives valuable information about the rotation of the nucleotides within the nanopore. Employing the above-mentioned semiquantitative parameters, we first try to assess the interaction of different nucleotides with graphene as well as G/h-BN nanopores in a vacuum. Then, we will consider the essential impact of the solvent environment on the interaction and show how the aqueous environment will change the dynamic behavior of the nucleotides within different nanopores.

● **Nucleotide/nanopore interaction in vacuum**

In the first step, we examined the interaction of different nucleotides with a pure graphene nanopore. The metrics for these interactions are shown in Fig. 4(a)–(c). There is a distinct difference between the dynamic behavior of purines (dAMP and dGMP)

and pyrimidines (dCMP and dTMP) nucleotides. While purines have shown a high tendency to leave the nanopore, pyrimidines show strong H-bonds toward the nanopore edges and prefer to stay within the nanopore. This behavior can be attributed to the different molecular structures, particularly different sizes, of purines and pyrimidines as decisive factors. Purines have a two-ringed molecular structure in contrast to single-ringed pyrimidines. The larger size of purines makes them more susceptible to the electrostatic repulsive force by nanopores and caused their outward movement. Fig. 4(b) and (c) shows the minimum distance between the electronegative ends/backbone of the nucleotides and the nanopore edges. It is interesting to note that as the backbone of dGMP leaves the nanopore, the hydrogen bond between the electronegative end of dGMP (O) and the nanopore edge tries to keep the nucleotide within the nanopore. On the other hand, the interaction between the electronegative end and the nanopore edges in dAMP (N) is not strong enough to hold the nucleotide, therefore dAMP leaves the nanopore while rotating around its axis. The higher electronegativity of oxygen (3.44) compared to that of nitrogen (3.04) could be an explanation for this different behavior. In contrast to purines, the smaller pyrimidines stay within the nanopore by maintaining the H-bonds between their electronegative ends and nanopore edge in most of the AIMD simulation time. Among all nucleotides, dCMP shows the strongest interaction with nanopore edges due to the presence of two anchoring electronegative sites (O and N) in its molecular structure.
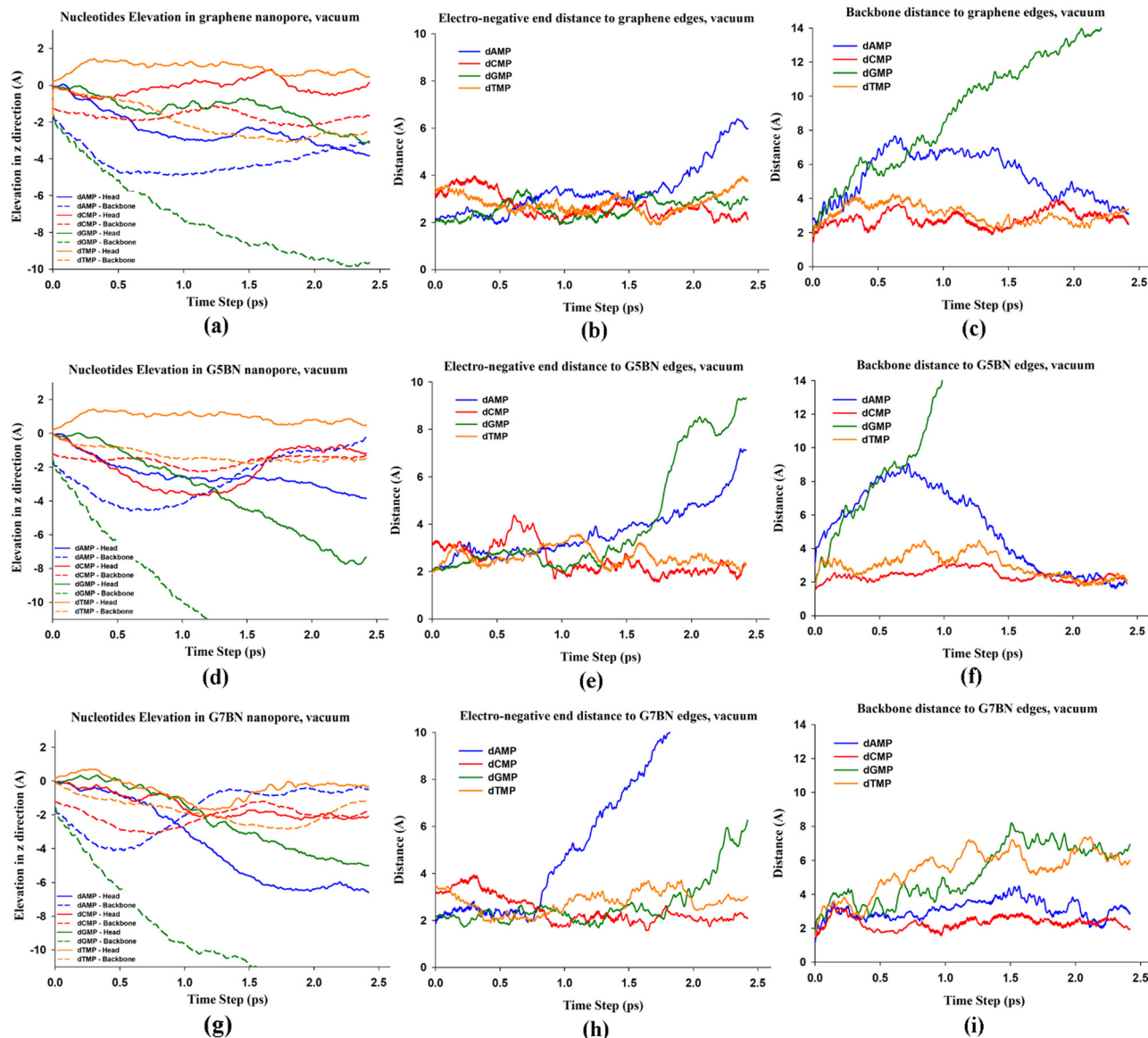
13456 | *Phys. Chem. Chem. Phys.*, 2023, **25**, 13452–13464

This journal is © the Owner Societies 2023

Fig. 4 The elevation of nucleotides in (a) graphene, (d) G5BN), and (g) G7BN nanopores. The head of the nucleotide is plotted straight, and the backbone is plotted in dashed lines. The minimum distance between the active ends of nucleotides and hydrogen in (b) graphene, (e) G5BN, and (h) G7BN nanopore edges. The minimum distance between the oxygen of the backbone and hydrogen in (c) graphene, (f) G5BN, (i) and G7BN nanopore edges.

The data in Fig. 4(c) show that, while the backbone of pyrimidines stays in the range between 2–4 Å from the nanopore edge, the backbone of purines is repelled from the edges. Although the backbone of dAMP reaches an average distance of about 4 Å at the final time steps, the backbone of dGMP moves away and leads to an outward displacement of this nucleotide.

The general behavior of nucleotides in G/h-BN nanopores is similar to their dynamic pattern in a pure graphene nanopore. While purines tend to leave the nanopore, the pyrimidines hold their position by maintaining H-bonds with G/h-BN nanopore edges. However, comparing the elevation graph in the z-direction, which is plotted in Fig. 4(d) and (g), reveals that the G/h-BN nanopores push out the purines faster than the graphene nanopore. In the graphene nanopore, the electronegative end of dGMP managed to maintain the bond with the

edge throughout the simulation, while the backbone is pushed outward at a 55 Å ps^{-1} rate. In contrast, in the G/h-BN nanopores, the backbone of dGMP was pushed out at the rate of 80 Å ps^{-1} and the hydrogen bonds with the nanopore edge finally breaks. This behavior indicates that the G/h-BN nanopores cause stronger repulsive forces at the backbone of the nucleotides compared with the pure graphene nanopore.

Also, the results indicate that the interaction of the nucleotide with either pure graphene or G/h-BN nanopores heavily relies on their molecular structure. We observed that dAMP maintains its bond with graphene nanopore edges for a longer time than is the case in the G5BN and G7BN nanopores. For further clarification, the average distance between the active ends of nucleotides and the nearest atoms of nanopore edges throughout the simulation is extracted and presented in

This journal is © the Owner Societies 2023

Phys. Chem. Chem. Phys., 2023, **25**, 13452–13464 | **13457**

Table 1 Average distance between electronegative ends of nucleotides and nanopore edges in vacuum system

| El. ends	dAMP	dCMP	dGMP	dTMP
G0BN	3.381	2.697	2.592	2.803
G5BN	3.649	2.501	4.086	2.623
G7BN	4.590	2.512	2.702	2.527

Table 1. The average distance between the electronegative end of dAMP and graphene, G5BN, and G7BN nanopore edges are 3.38, 3.64, and 4.59 Å, respectively. These values show the stronger interaction between the electronegative end (N) of dAMP and graphene nanopore compared to the G/h-BN ones. This behavior can be explained by the stronger bond between the nitrogen atom in the dAMP structure and the hydrogen-terminated carbon atoms, compared to the interaction with hydrogen-terminated nitrogen or boron atoms at the edge of the G/h-BN nanopores. This analysis reveals that the strength of the H-bonds depends on the type of atoms at the electronegative end of the nucleotides as well as the atoms at the nanopore edge.

In contrast to the dAMP, the dGMP has an oxygen electronegative end. In this case, the H-bond in G/h-BN nanopores with hydrogen-terminated nitrogen at the edge is much stronger than the H-bond in graphene. Nevertheless, the formed hydrogen bond is insufficient to neutralize the strong repulsive force on the backbone caused by G/h-BN nanopores, and dGMP is pushed out of the nanopore (Table 2). It should be noted that no stable H-bond between B–H edges in G/h-BN nanopores and electronegative ends (O or N) has been observed. We should also mention that the nanopore edges in G7BN consist of B–H and N–H edges while some parts of the G5BN nanopore edge have C–H edges. Therefore, due to the stronger interaction of the O-end of the nucleotide with the N–H rather than the C–H edge, the H-bond for dGMP seems to be stronger in the G7BN nanopore. In contrast to the purines, the pyrimidines (dCMP and dTMP) maintain their horizontal orientation and stay in the G/h-BN nanopores. The active ends of dCMP and dTMP move toward the nanopore edges and form a strong H-bond, which is maintained throughout the simulation time.

Fig. 5 depicts the local density of states (LDOS) of dCMP and dGMP placed in the G5BN nanopore in the middle and final stages of the simulation. Also, the differential local charge density (dRHO) for the mentioned systems is plotted in Fig. S5 (ESI†). The snapshots were chosen at specific time steps to clearly illustrate the impact of the nucleotides on the electronic structure of the nanopores throughout the simulation. During the initial up to the middle steps of the simulation, the distance

Table 2 Average distance between the oxygen of backbone and nanopore edges in vacuum system

Backbone	dAMP	dCMP	dGMP	dTMP
G0BN	5.328	2.810	9.434	3.088
G5BN	5.890	2.384	12.265	2.978
G7BN	4.447	2.213	12.382	2.415

dCMP

Mid steps   Final steps

dGMP
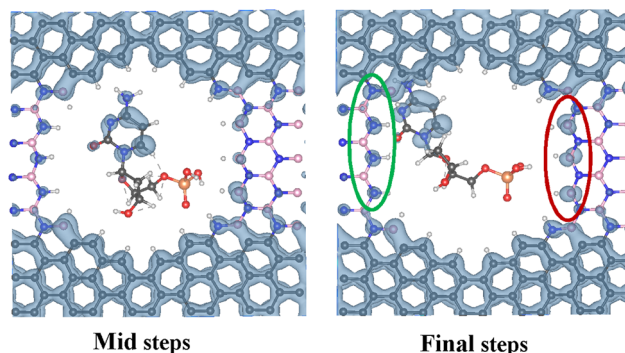
Mid steps   Final steps
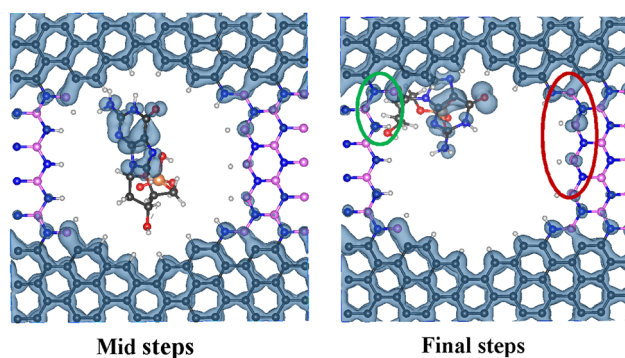
Fig. 5 Local density of states (LDOS) for G5BN in the presence of dCMP and dGMP.

between the active ends of dCMP and the nanopore edges is larger than 4 Å, with no significant interaction, as shown in Fig. 5. At the final steps however, the active end of dCMP manages to reach the nanopore edge and to form a hydrogen bond. The influence of their interaction with the nanopore edge (h-BN edge of the nanopore) is highlighted in green in Fig. 5. In addition, the interaction between the backbone of dCMP and the edge on the other side of the nanopore leads to the modulation in the density of the local states (highlighted in red). On the other hand, the active end of dGMP formed a bond with the edges in the initial steps of the simulation. However, the bond is ultimately broken in the final steps of the simulation, see the LDOS in Fig. 5.

The distance between the active ends of nucleotides and the nanopore edges corresponds to their interaction and the strength of the bond between nucleotides and nanopores. Therefore, the average distances can be considered as a reasonable quantity to extrapolate the average interaction strength between nucleotides and nanopores. On the basis of this analysis, the interaction strength between the active ends of nucleotides and nanopore edges can be ordered as G > C > T > A, C > T > A > G, and C > T > G > A for graphene, G5BN, and G7BN, respectively. The result indicates that dCMP has the strongest interaction with the nanopore edges compared to the other nucleotides. Comparing the average distances between the nucleotide and the edge of the graphene and G/h-BN nanopores reveals that the main essential factor is

13458 | *Phys. Chem. Chem. Phys.,* 2023, **25**, 13452–13464

This journal is © the Owner Societies 2023

related to the different atoms or complexes at the edge of the nanopores (C–H, N–H, and B–H). It is also concluded that the electronegative end of purines has a higher tendency to interact with graphene nanopores, while the electronegative ends of pyrimidines make a stronger bond with G/h-BN nanopores.

Contrary to the different interaction patterns for electronegative ends and nanopore edges, the average distances between the backbones and nanopore edges show a similar pattern as G > A > T > C for all nanopores. This behavior indicates that the backbone interaction is strongly correlated to the size of the nucleotides instead of interaction with different atoms in nanopore edges. In other words, there is no attractive interaction between the backbone and different atoms at the edge of nanopores to anchor the nucleotides within the nanopores.

● **Nucleotide/nanopore interaction in the aqueous environment**

In order to obtain a more realistic picture of the nucleotide interaction and dynamics within the nanopores, all calculations are repeated in the aqueous environment. The supercells are filled with water molecules modelling the density of pure water at atmospheric pressure and ambient temperature (1 g cm^{-3}). During the whole simulation time, the water molecules show their natural Brownian motion, with no tendency to interact with nanopore edges or nucleotides, therefore, no reaction has been observed and the whole system remains stable. Fig. 6 depicts the snapshots of dCMP and dGMP interaction with the G7BN nanopore in a solvent environment throughout the simulation time. Similar snapshots for dAMP and dTMP in a G7BN nanopore are plotted in Fig. S6 (ESI†).

In contrast to the calculations in a vacuum, Fig. 6 shows that the dGMP nucleotide remains within the nanopore for the whole calculation time. This can be attributed to the existing water molecules, which hinder the free movement of the nucleotides. The same picture is also observed for the other purine base, dAMP. More details on this effect are revealed by a direct comparison of the average perpendicular (z-direction) movement of the nucleotides in an aqueous environment (left panels of Fig. 7) and a vacuum environment (left panels of Fig. 4). The comparison shows that the presence of water molecules clearly blocks the out of the plane motion of purines. For instance, dGMP tends to stay in graphene and G5BN nanopores, and its backbone speed in the G7BN nanopore is decreased from 80 Å ps^{-1} in the vacuum to 30 Å ps^{-1} in the solvent environment.

The stabilizing effect of water molecules is also reflected in the average distance of the backbone and nanopore edges. Table 3 shows these average values in an aqueous environment. Comparing these results with the results of the vacuum case indicates that the distance between the backbone of dGMP is decreased by 6.205, 9.105, and 7.139 Å due to the presence of water molecules, in graphene, G5BN, and G7BN nanopores, respectively. The same effect is observed for dAMP, where the average distances are reduced by 2.323, 1.992, and 1.348 Å in graphene, G5BN, and G7BN nanopores, respectively.

dCMP

Initial steps   Mid steps   Final steps

dGMP

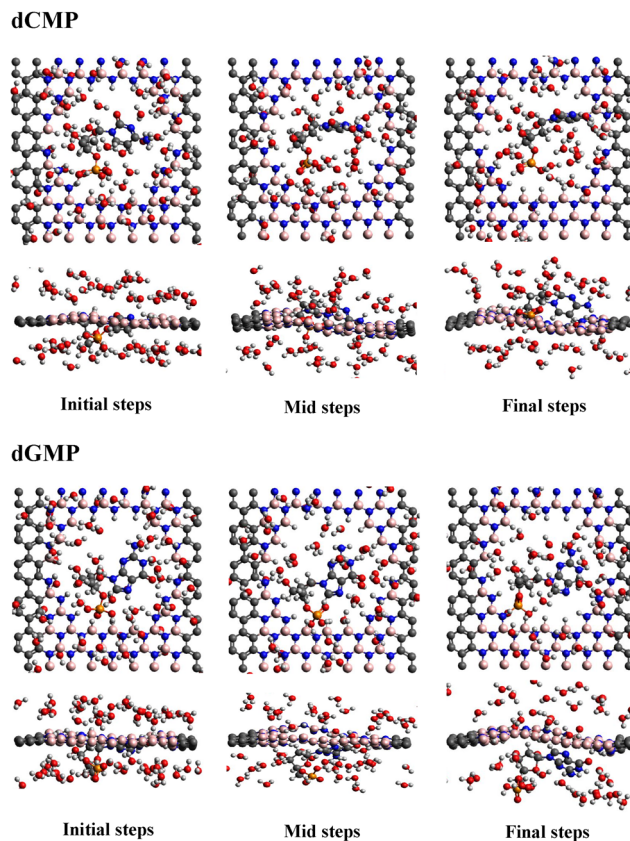Initial steps   Mid steps   Final steps

Fig. 6 dCMP and dGMP interaction with G7BN nanopore in the initial, middle, and final steps of AIMD simulation in the solvent environment.

The average distances between electronegative ends and nanopore edges in an aqueous environment are listed in Table 4. The comparison of these values with the results in Table 1 shows that the interactions of the electronegative ends of the pyrimidine bases in a solvent environment are almost similar to their interactions in a vacuum environment. The H-bonds are preserved between the electronegative ends of dTMP and nanopore edges even in the aqueous environment. However, we observed the breaking of hydrogen bonds for dCMP in some instances. Comparing the right panels of Fig. 7 (aqueous) and Fig. 4 (vacuum) confirms the above statement. Although dCMP shows a relatively stable and strong H-bond toward the edges of all three nanopores in a vacuum, the interactions are weakened in the solvent environment. Fig. 7 shows that the H-bond between the electronegative end of dCMP and the G7BN nanopore breaks several times during the simulation. The average distance for dCMP in G7BN increases by 2.293 Å due to the water molecules. In the case of an aqueous environment, the presence of water molecules within the nanopore leads to the screening effect, which in turn reduces the interaction between the electronegative end of the nucleotides and the nanopore edge. In the case of dCMP, the small size of the nucleotide also provides more space for water molecules within the nanopore. Moreover, the hydrophilic Character of the h-BN edge in G7BN increases the number of water molecules between the electronegative ends of dCMP and
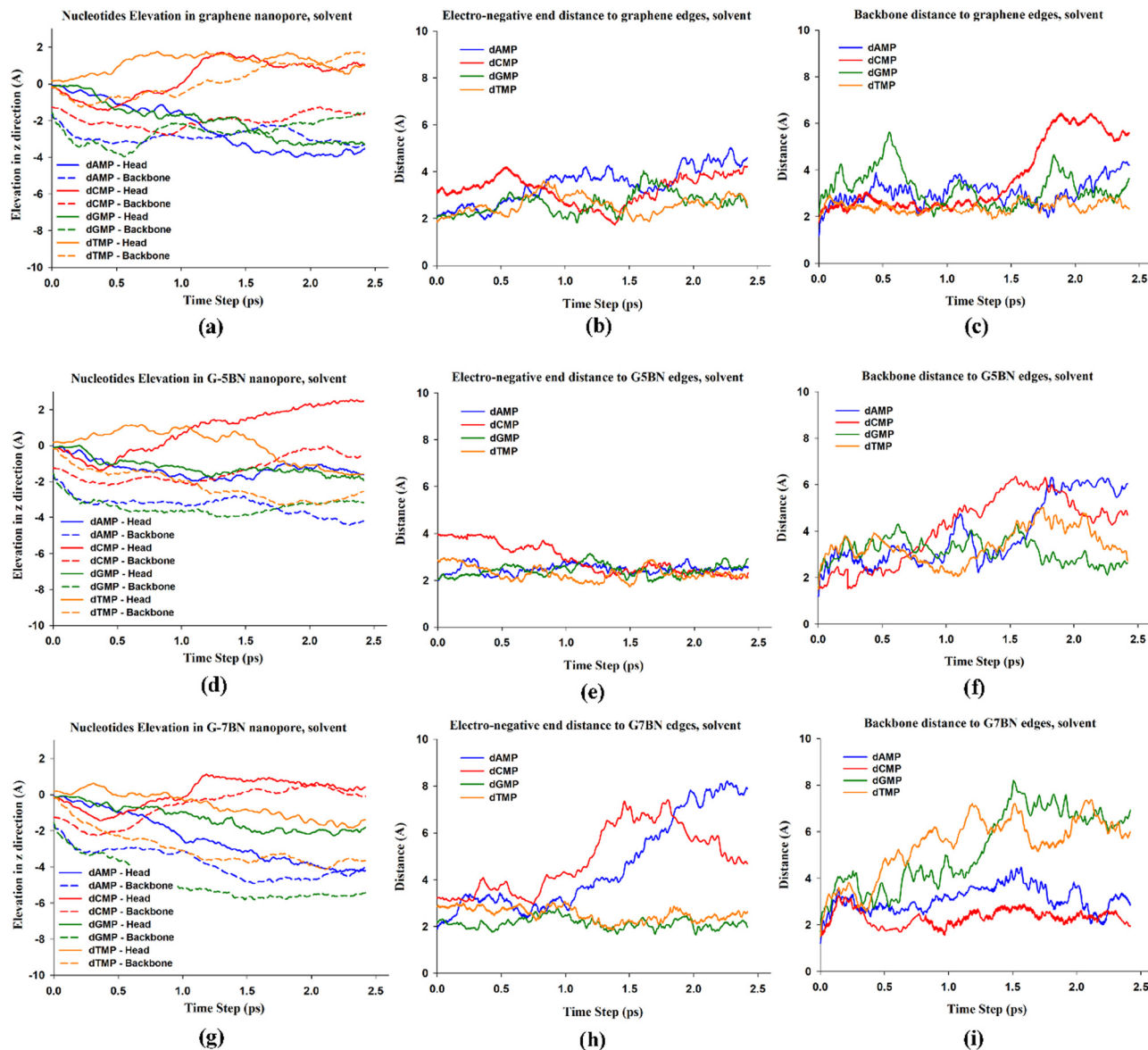
This journal is © the Owner Societies 2023

Phys. Chem. Chem. Phys., 2023, **25**, 13452–13464 | **13459**

Fig. 7 The geometric parameters in the solvent environment. The elevation of nucleotides in (a) graphene, (d) G5BN, and (g) G7BN nanopores. The head of the nucleotide is plotted straight, and the backbone is plotted in dashed lines. The minimum distance between the electronegative active ends of nucleotides and passivating hydrogen in (b) graphene, (e) G5BN, and (h) G7BN nanopores. The minimum distance between the oxygen of the backbone and hydrogen in (c) graphene, (f) G5BN, (i) and G7BN nanopore edges.

Table 3 Average distance between the oxygen of backbone and nanopore edges in the solvent environment

Backbone	dAMP	dCMP	dGMP	dTMP
G0BN	3.045	3.656	3.229	2.419
G5BN	3.898	4.143	3.160	3.399
G7BN	3.099	2.316	5.243	5.429

Table 4 Average distance between electronegative ends of nucleotides and nanopore edges in solvent environment

El. ends	dAMP	dCMP	dGMP	dTMP
G0BN	3.443	3.232	2.660	2.592
G5BN	2.481	2.909	2.431	2.292
G7BN	3.985	4.805	2.158	2.548

the nanopore edge in G7BN, which in turn leads to the strong screening and finally the breakdown of H-bonds (for simulation times > 0.10 ps). We should note that, while dTMP has two highly electronegative O atoms as electronegative ends, the dCMP nucleotide has one O and one less electronegative N atom.

This difference is also reflected in the dynamics of the two pyrimidines. While the dTMP bonds with edges formed in the first 1000 steps of simulation, dCMP requires around 18 000 simulation steps to reach the edges of the G7BN nanopore. This explains, why the dCMP is more susceptible to the screening effect.

To further investigate the interaction between dCMP and the G7BN nanopore in a solvent environment, the AIMD simulation was conducted with an initial temperature of 350 K. The results have indicated that nucleotides, G/h-BN/G nanopore, and water molecules remained stable throughout the simulation with the raised temperature. Fig. S7 (ESI†) shows the snapshots of dCMP and dGMP within the G7BN nanopore in a solvent environment with an initial temperature of 350 K. Also, the minimum distance between the active ends and the backbones of the nucleotides toward the nanopore edges is illustrated in Fig. S8 (ESI†). The results indicate that raising the temperature has little impact on the motion of dGMP and its interaction with the G7BN nanopore. However, the higher kinetic energy of dCMP caused by raising the temperature to 350 K helps the nucleotide to overcome the resistance caused by water molecules. Hence, dCMP managed to reach the nanopore edges, and the active ends of dCMP formed a strong bond with the G7BN nanopore.

The stabilization of the larger purines within the nanopores leads to a general reduction of the distance between the electronegative ends of these nucleotides and nanopore edges. The average values are listed in Table 4 for the aqueous environment. Comparing these values with the results in Table 1 (vacuum) reveals that in almost all the cases the average distances are reduced. However, Fig. 7 shows that the distance between the electronegative ends (N) of dAMP and G7BN nanopore rapidly increases in the second half of the simulation time. Apart from the screening effect of the water molecule, there are several important factors that lead to this observation. First of all, we should note that the dAMP nucleotide has an N atom as its electronegative end rather than O, which builds a weaker bonding to the nanopore edge due to its lower electronegativity. Second, the N electronegative atom shows weaker interaction with the B–H and N–H edges of the G7BN nanopore compared to the C–H edges in the graphene nanopore. Moreover, the hydrophilicity of h-BN leads to more water molecules within the G7BN nanopore and more screening. All these effects result in a large distance between the electronegative end of dAMP and the nanopore edge in the G7BN structure. In contrast to dAMP, the dGMP nucleotide shows a strong H-bond in all three nanopores. This can be explained by the stronger interaction of O atoms as the electronegative end of dGMP with both C–H and N–H edges.

The nanopore technology has been employed in DNA sequencing considering two different effects. One is related to the translocation dynamics of the nucleotides within the nanopore and the consequent modulation in the ionic current through the nanopore. The second effect is related to the modulation of the electronic current on the surface of a two-dimensional membrane, where the interaction between the nucleotides and the nanopore edge results in a modulation of electronic current. Therefore, it is also essential to evaluate the interaction energy or binding energy of each nucleotide within the different nanopores as a factor, which determines the changes in the electronic structure and consequently electronic current of the membranes. The binding energies between nucleotides and different nanopores in vacuum and aqueous environments are calculated according to eqn (1) and plotted in Fig. 8. It should be noted that water molecules have been removed before calculating the binding energy in the aqueous environment. Thus the binding energies only include the interaction between nucleotides and nanopore structures.

The energies can be calculated for any snapshot during the simulation time. We chose two separate snapshots, where the first snapshot corresponds to the middle of the simulation time in which the nucleotides are still moving toward the stable geometry, and the second snapshot is related to the final stage. In the vacuum environment, the pyrimidine bases show strong binding with the nanopores. The binding energy of dTMP toward all three nanopores is around 0.5 eV, which indicates the formation of hydrogen bonds. Also, dCMP shows the strongest binding toward G/h-BN nanopores, resulting from the strong interaction between two active ends and nanopore edges. On the contrary, the tendency of the purine bases to leave the nanopore is reflected by their binding energies. For example, the electronegatively-active end of the dGMP
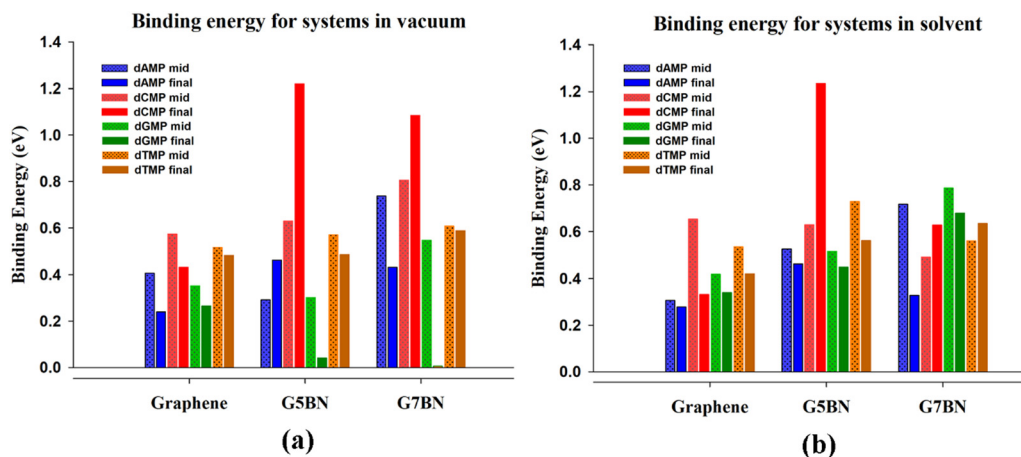

Fig. 8 The binding energies of the nucleotides to the graphene and G/h-BN nanopores in: (a) vacuum environment (b) solvent environment.

maintains the bond with G-5BN and G-7BN nanopore edges till the middle of the simulation, however, the bond is broken during the final steps and this leads to zero binding energies.

As shown previously, the purine bases maintain their bonds with the nanopores in the presence of water molecules. The binding energies confirm this behavior, where dGMP and dAMP show strong binding energy with G/h-BN nanopores even at the final steps of the simulation. These results clearly show that the aqueous environment has a non-negligible effect on the nucleotide-nanopore interaction. This fact puts a question mark on previous theoretical works, which did not consider the effect of solvent in their modeling. As a rough estimation, if we consider the interaction energies as a factor to detect or to sequence different nucleotides, our results generally show that the aqueous environment makes the nucleotides less distinguishable. Considering the G5BN nanopore, where the interaction energies show larger variations, the dCMP nucleotide and to a certain extent the dTMP nucleotide can be distinguished, while the purine bases (dAMP and dGMP) show very similar interaction energies. Another conclusion that can be extracted from these results is the advantage of hybrid nanopores (G5BN and G7BN) over the pure graphene nanopore. These nanopores generally show higher interactions with different nucleotides, which is a positive point in both ionic and electronic current sequencing techniques.

Conclusion

We have investigated the interaction between nucleotides of the DNA strands and nanopores in G/h-BN/G heterostructures to evaluate their aptitude for DNA sequencing applications. Car-Parrinello molecular dynamics (CPMD), which is a DFT-based *ab initio* molecular dynamics method, is employed to dynamically simulate the interactions in a vacuum as well as in an aqueous environment. The nucleotide/nanopore interaction in a vacuum environment indicates that purine bases have a higher tendency to leave the nanopore. This behavior is caused by their larger size, making them more susceptible to the electrostatic repulsive force of nanopores. On the contrary, the pyrimidine bases have maintained their position in graphene and G/h-BN nanopores while their electronegative active ends form strong H-bonds with nanopore edges. Also, it has been revealed that different atoms at the edge of the nanopores (C–H, N–H, and B–H) have a crucial impact on the interaction with nucleotides. Furthermore, the average distances between the backbone and different nanopore edges follow a similar pattern, illustrating that their interaction is more relying on the size of the nucleotides.

Simulating the nucleotide/nanopore interaction in a solvent environment shows that water molecules have no tendency to form bonds with nucleotide or nanopore structures. However, their presence has a significant impact on the motion of nucleotides and their interaction with nanopore edges. While the presence of water molecules helps purine bases to maintain their position in the nanopore, their screening effect weakens the interaction of the electronegative ends with nanopore edges in pyrimidines. Also, the calculated binding energy between nucleotides and nanopores shows that filling the supercell with water molecules has a non-negligible effect on the interaction and makes the discrimination more challenging. Also, it has been shown that G/h-BN nanopores have generally stronger interactions with different nucleotides compared to graphene nanopores.

Conflicts of interest

There are no conflicts to declare.

Acknowledgements

References

1 E. R. Mardis, A Decade's Perspective on DNA Sequencing Technology, *Nature*, 2011, **470**(7333), 198–203, DOI: **10.1038/nature09796**.

2 B. M. Venkatesan and R. Bashir, Nanopore Sensors for Nucleic Acid Analysis, *Nat. Nanotechnol.*, 2011, **6**(10), 615–624, DOI: **10.1038/nnano.2011.129**.

3 J. J. Kasianowicz, Flossing with DNA, *Nat. Mater.*, 2004, **3**(6), 355–356, DOI: **10.1038/nmat1143**.

4 H. Chang, F. Kosari, G. Andreadakis, M. A. Alam, G. Vasmatzis and R. Bashir, DNA-Mediated Fluctuations in Ionic Current through Silicon Oxide Nanopore Channels, *Nano Lett.*, 2004, **4**(8), 1551–1556, DOI: **10.1021/nl049267c**.

5 M. Venkatesan, S. Yemenicioglu, B. Dorvel and R. Bashir, Fabrication and Characterization of Tunable, Low Stress Al_2O_3 Nanopores for the Electronic Detection of Biomolecules, *Biophys. J.*, 2009, **96**(3), 645a, DOI: **10.1016/j.bpj.2008.12.3838**.

6 J. Shim, J. A. Rivera and R. Bashir, Electron Beam Induced Local Crystallization of HfO_2 Nanopores for Biosensing Applications, *Nanoscale*, 2013, **5**(22), 10887, DOI: **10.1039/c3nr02608f**.

7 J. B. Heng, A. Aksimentiev, C. Ho, P. Marks, Y. V. Grinkova, S. Sligar, K. Schulten and G. Timp, Stretching DNA Using the Electric Field in a Synthetic Nanopore, *Nano Lett.*, 2005, **5**(10), 1883–1888, DOI: **10.1021/nl0510816**.

8 Z. Yuan, C. Wang, X. Yi, Z. Ni, Y. Chen and T. Li, Solid-State Nanopore, *Nanoscale Res. Lett.*, 2018, **13**, 56, DOI: **10.1186/s11671-018-2463-z**.

9 N. Yang and X. Jiang, Nanocarbons for DNA Sequencing: A Review, *Carbon*, 2017, **115**, 293–311, DOI: **10.1016/j.carbon.2017.01.012**.

13462 | *Phys. Chem. Chem. Phys.*, 2023, **25**, 13452–13464

This journal is © the Owner Societies 2023

10 K. Liu, M. Lihter, A. Sarathy, S. Caneva, H. Qiu, D. Deiana, V. Tileli, D. T. L. Alexander, S. Hofmann, D. Dumcenco, A. Kis, J.-P. Leburton and A. Radenovic, Geometrical Effect in 2D Nanopores, *Nano Lett.*, 2017, **17**(7), 4223–4230, DOI: **10.1021/acs.nanolett.7b01091**.

11 Q. Xu, M.-Y. Wu, G. F. Schneider, L. Houben, S. K. Malladi, C. Dekker, E. Yucelen, R. E. Dunin-Borkowski and H. W. Zandbergen, Controllable Atomic Scale Patterning of Free-standing Monolayer Graphene at Elevated Temperature, *ACS Nano*, 2013, **7**(2), 1566–1572, DOI: **10.1021/nn3053582**.

12 C. A. Merchant, K. Healy, M. Wanunu, V. Ray, N. Peterman, J. Bartel, M. D. Fischbein, K. Venta, Z. Luo, A. T. C. Johnson and M. Drndić, DNA Translocation through Graphene Nano-pores, *Nano Lett.*, 2010, **10**(8), 2915–2921, DOI: **10.1021/nl101046t**.

13 A. Wasfi, F. Awwad and A. I. Ayesh, Graphene-Based Nano-pore Approaches for DNA Sequencing: A Literature Review, *Biosens. Bioelectron.*, 2018, **119**, 191–203, DOI: **10.1016/j.bios.2018.07.072**.

14 J. Feng, K. Liu, R. D. Bulushev, S. Khlybov, D. Dumcenco, A. Kis and A. Radenovic, Identification of Single Nucleotides in MoS_2 Nanopores, *Nat. Nanotechnol.*, 2015, **10**(12), 1070–1076, DOI: **10.1038/nnano.2015.219**.

15 S.-M. Tabatabaei, M. Pourfath and M. Fathipour, Adsorp-tion Characteristics of Epigenetically Modified DNA Nucleo-bases on Single-Layer MoS_2: A First-Principles Study, *J. Appl. Phys.*, 2018, **124**(13), 134501, DOI: **10.1063/1.5034004**.

16 J.-H. Lee, Y.-K. Choi, H.-J. Kim, R. H. Scheicher and J.-H. Cho, Physisorption of DNA Nucleobases on H-BN and Graphene: VdW-Corrected DFT Calculations, *J. Phys. Chem. C*, 2013, **117**(26), 13435–13441, DOI: **10.1021/jp402403f**.

17 S. J. Heerema and C. Dekker, Graphene Nanodevices for DNA Sequencing, *Nat. Nanotechnol.*, 2016, **11**(2), 127–136, DOI: **10.1038/nnano.2015.307**.

18 R. L. Kumawat and B. Pathak, Identifying DNA Nucleotides via Transverse Electronic Transport in Atomically Thin Topologically Defected Graphene Electrodes, *ACS Appl. Bio Mater.*, 2020, **4**(2), 1403–1412, DOI: **10.1021/acsabm.0c01309**.

19 G. F. Schneider, S. W. Kowalczyk, V. E. Calado, G. Pandraud, H. W. Zandbergen, L. M. K. Vandersypen and C. Dekker, DNA Translocation through Graphene Nanopores, *Nano Lett.*, 2010, **10**(8), 3163–3167, DOI: **10.1021/nl102069z**.

20 Y. Yu, X. Lu, H. Ding and Y. Ma, Computational Investiga-tion on DNA Sequencing Using Functionalized Graphene Nanopores, *Phys. Chem. Chem. Phys.*, 2018, **20**(14), 9063–9069, DOI: **10.1039/c7cp07462j**.

21 S. J. Heerema, G. F. Schneider, M. Rozemuller, L. Vicarelli, H. W. Zandbergen and C. Dekker, 1/F Noise in Graphene Nanopores, *Nanotechnology*, 2015, **26**(7), 074001, DOI: **10.1088/0957-4484/26/7/074001**.

22 G. F. Schneider, Q. Xu, S. Hage, S. Luik, J. N. H. Spoor, S. Malladi, H. Zandbergen and C. Dekker, Tailoring the Hydrophobicity of Graphene for Its Use as Nanopores for DNA Translocation, *Nat. Commun.*, 2013, **4**, 2619, DOI: **10.1038/ncomms3619**.

23 D. G. Sangiovanni, R. Faccio, G. K. Gueorguiev and A. Kakanakova-Georgieva, Discovering Atomistic Pathways for Supply of Metal Atoms from Methyl-Based Precursors to Graphene Surface, *Phys. Chem. Chem. Phys.*, 2023, **25**(1), 829–837, DOI: **10.1039/d2cp04091c**.

24 F. A. L. de Souza, R. G. Amorim, W. L. Scopel and R. H. Scheicher, Nano-Structured Interface of Graphene and H-BN for Sensing Applications, *Nanotechnology*, 2016, **27**(36), 365503, DOI: **10.1088/0957-4484/27/36/365503**.

25 Q. Li, M. Liu, Y. Zhang and Z. Liu, Hexagonal Boron Nitride-Graphene Heterostructures: Synthesis and Interfacial Proper-ties, *Small*, 2015, **12**(1), 32–50, DOI: **10.1002/smll.201501766**.

26 R. J. P. Román, F. J. R. C. Costa, A. Zobelli, C. Elias, P. Valvin, G. Cassabois, B. Gil, A. Summerfield, T. S. Cheng, C. J. Mellor, P. H. Beton, S. V. Novikov and L. F. Zagonel, Band Gap Measurements of Monolayer H-BN and Insights into Carbon-Related Point Defects, *2D Mater.*, 2021, **8**(4), 044001, DOI: **10.1088/2053-1583/ac0d9c**.

27 S. Liu, B. Lu, Q. Zhao, J. Li, T. Gao, Y. Chen, Y. Zhang, Z. Liu, Z. Fan, F. Yang, L. You and D. Yu, Boron Nitride Nanopores: Highly Sensitive DNA Single-Molecule Detectors, *Adv. Mater.*, 2013, **25**(33), 4549–4554, DOI: **10.1002/adma.201301336**.

28 Z. Zhou, Y. Hu, H. Wang, Z. Xu, W. Wang, X. Bai, X. Shan and X. Lu, DNA Translocation through Hydrophilic Nano-pore in Hexagonal Boron Nitride, *Sci. Rep.*, 2013, **3**, 3287, DOI: **10.1038/srep03287**.

29 J. S. Lee, J. P. Oviedo, Y. M. N. D. Bandara, X. Peng, L. Xia, Q. Wang, K. Garcia, J. Wang, M. J. Kim and M. J. Kim, Detection of Nucleotides in Hydrated SsDNA via 2D H-BN Nanopore with Ionic-Liquid/Salt–Water Interface, *Electrophoresis*, 2021, **42**(7–8), 991–1002, DOI: **10.1002/elps.202000356**.

30 S. Gbadamasi, M. Mohiuddin, V. Krishnamurthi, R. Verma, M. W. Khan, S. Pathak, K. Kalantar-Zadeh and N. Mahmood, Interface Chemistry of Two-Dimensional Hetero-structures – Fundamentals to Applications, *Chem. Soc. Rev.*, 2021, **50**(7), 4684–4729, DOI: **10.1039/D0CS01070G**.

31 V. Shukla, N. K. Jena, A. Grigoriev and R. Ahuja, Prospects of Graphene–HBN Heterostructure Nanogap for DNA Sequen-cing, *ACS Appl. Mater. Interfaces*, 2017, **9**(46), 39945–39952, DOI: **10.1021/acsami.7b06827**.

32 F. A. L. de Souza, G. Sivaraman, M. Fyta, R. H. Scheicher, W. L. Scopel and R. G. Amorim, Electrically Sensing Hachi-moji DNA Nucleotides through a Hybrid Graphene/*H*-BN Nanopore, *Nanoscale*, 2020, **12**(35), 18289–18295, DOI: **10.1039/d0nr04363j**.

33 A. Kiakojouri, I. Frank and E. Nadimi, In-Plane Graphene/H-BN/Graphene Heterostructures with Nanopores for Elec-trical Detection of DNA Nucleotides, *Phys. Chem. Chem. Phys.*, 2021, **23**(44), 25126–25135, DOI: **10.1039/d1cp03597e**.

34 A. Tyagi, K. Chu, M. D. Hossain, I. H. Abidi, W. Lin, Y. Yan, K. Zhang and Z. Luo, Revealing the Mechanism of DNA Passing through Graphene and Boron Nitride Nanopores, *Nanoscale*, 2019, **11**(48), 23438–23448, DOI: **10.1039/c9nr07651d**.

35 A. Smolyanitsky and B. Luan, Nanopores in Atomically Thin 2D Nanosheets Limit Aqueous Single-Stranded DNA

Transport, *Phys. Rev. Lett.*, 2021, **127**(13), 138103, DOI: 10.1103/physrevlett.127.138103.

36 C. Huang, X. Zhu, Z. Li, X. Ma, N. Li, J. Luo and J. Fan, Molecular Insights into Geometric and Electrophoretic Effects on DNA Translocation Speed through Graphene Nanoslit Sensor, *Carbon*, 2022, **191**, 415–423, DOI: 10.1016/j.carbon.2022.01.068.

37 G. T. Feliciano, C. Sanz-Navarro, M. D. Coutinho-Neto, P. Ordejón, R. H. Scheicher and A. R. Rocha, Addressing the Environment Electrostatic Effect on Ballistic Electron Transport in Large Systems: A QM/MM-NEGF Approach, *J. Phys. Chem. B*, 2017, **122**(2), 485–492, DOI: 10.1021/acs.jpcb.7b03475.

38 I. Rungger, X. Chen, U. Schwingenschlögl and S. Sanvito, Finite-Bias Electronic Transport of Molecules in a Water Solution, *Phys. Rev. B: Condens. Matter Mater. Phys.*, 2010, **81**(23), 235407, DOI: 10.1103/physrevb.81.235407.

39 R. Car and M. Parrinello, Unified Approach for Molecular Dynamics and Density-Functional Theory, *Phys. Rev. Lett.*, 1985, **55**(22), 2471–2474, DOI: 10.1103/physrevlett.55.2471.

40 CPMD. Copyright IBM Corp, 1990–2008; Copyright MPI für Festkörperforshung Stuttgart 1997–2001. Available online: https://www.cpmd.org/ (accessed on 16 January 2012).

41 N. Troullier and J. L. Martins, Efficient Pseudopotentials for Plane-Wave Calculations, *Phys. Rev. B: Condens. Matter*

Mater. Phys., 1991, **43**(3), 1993–2006, DOI: 10.1103/physrevb.43.1993.

42 J. P. Perdew, K. Burke and M. Ernzerhof, Generalized Gradient Approximation Made Simple, *Phys. Rev. Lett.*, 1996, **77**(18), 3865–3868, DOI: 10.1103/physrevlett.77.3865.

43 S. Grimme, Semiempirical GGA-Type Density Functional Constructed with a Long-Range Dispersion Correction, *J. Comput. Chem.*, 2006, **27**(15), 1787–1799, DOI: 10.1002/jcc.20495.

44 C. Lundgren, A. Kakanakova-Georgieva and G. K. Gueorguiev, A Perspective on Thermal Stability and Mechanical Properties of 2D Indium Bismide from Ab Initio Molecular Dynamics, *Nanotechnology*, 2022, **33**(33), 335706, DOI: 10.1088/1361-6528/ac6baf.

45 W. Humphrey, A. Dalke and K. Schulten, VMD: Visual Molecular Dynamics, *J. Mol. Graphics*, 1996, **14**(1), 33–38, DOI: 10.1016/0263-7855(96)00018-5.

46 M. Chen, H.-Y. Ko, R. C. Remsing, M. F. Calegari Andrade, B. Santra, Z. Sun, A. Selloni, R. Car, M. L. Klein, J. P. Perdew and X. Wu, Ab Initio Theory and Modeling of Water, *Proc. Natl. Acad. Sci. U. S. A.*, 2017, **114**(41), 10846–10851, DOI: 10.1073/pnas.1712499114.

47 J. M. Soler, E. Artacho, J. D. Gale, A. García, J. Junquera, P. Ordejón and D. Sánchez-Portal, The SIESTA Method for *Ab Initio* Order-*N* Materials Simulation, *J. Phys.: Condens. Matter*, 2002, **14**(11), 2745–2779, DOI: 10.1088/0953-8984/14/11/302.